



In vivo differentiation of common basal cell carcinoma subtypes by microvascular and structural imaging using dynamic optical coherence tomography

Lotte Themstrup^{1,2}  | Nathalie De Carvalho³  | Sabrina M. Nielsen⁴ | Jonas Olsen^{1,2} | Silvana Ciardo³ | Sandra Schuh⁵ | Birgit M.-H. Nørnberg⁶ | Julia Welzel⁵ | Martina Ulrich⁷ | Giovanni Pellacani³ | Gregor B. E. Jemec^{1,2}

¹Department of Dermatology, Zealand University Hospital, Roskilde, Denmark

²Faculty of Health and Medical Sciences, University of Copenhagen, Copenhagen, Denmark

³Department of Dermatology, University of Modena and Reggio Emilia, Modena, Italy

⁴Musculoskeletal Statistics Unit, The Parker Institute, Bispebjerg and Frederiksberg Hospital, Frederiksberg, Copenhagen, Denmark

⁵Department of Dermatology and Allergology, General Hospital Augsburg, Augsburg, Germany

⁶Department of Pathology, Zealand University Hospital, Roskilde, Denmark

⁷CMB/Collegium Medicum Berlin, Berlin, Germany

Correspondence

Lotte Themstrup, Department of Dermatology, Zealand University Hospital, Roskilde, Denmark.
Email: lotte.themstrup@gmail.com

Funding information

European Union's ICT Policy Support Program, Grant/Award Number: 621015; Oak Foundation, Grant/Award Number: OCAY-13-309

Abstract

The subtype of basal cell carcinoma (BCC) influences the choice of treatment. Optical coherence tomography (OCT) is a non-invasive imaging tool, and a recent development of an angiographic version of OCT has extended the application of OCT to image the cutaneous microvasculature (so-called dynamic OCT, D-OCT). This study explores D-OCT's ability to differentiate the common BCC subtypes by microvascular and structural imaging. Eighty-one patients with 98 BCC lesions, consisting of three subtypes: 27 superficial BCC (sBCC), 55 nodular BCC (nBCC) and 16 infiltrative BCC (iBCC) were D-OCT scanned at three European dermatology centres. Blinded evaluations of microvascular and structural features were performed, followed by extensive statistical analysis of risk ratio (RR) and multiple correspondence analysis. nBCC lesions displayed most characteristic structural and vascular features. Serpiginous vessels, branching vessels, vessels creating a circumscribed figure and sharply demarcated hyporeflective ovoid structures in the dermis were all associated with a higher risk of the subtype being nBCC. The presence of highly present lines and dark peripheral borders at the margin of ovoid structures was negatively associated with iBCC. Lastly, the finding of hyporeflective ovoid structures protruding from epidermis correlated with sBCC. We identified various microvascular and structural D-OCT features that may aid non-invasive identification of BCC subtypes. This would allow clinicians to individualize and optimize BCC treatment as well as aid follow-up of non-surgical treatment.

KEYWORDS

biophotonics, keratinocyte carcinoma, non-invasive imaging, non-melanoma skin cancer, OCT angiography

1 | INTRODUCTION

Basal cell carcinoma (BCC) is the most common cancer in Caucasians. The nodular BCC (nBCC) is the most common histopathological

subtype, but an increase in the proportion of superficial BCC (sBCC) and infiltrating BCC (iBCC) has been reported.^[1] Within recent years, several non-surgical treatments have been established for treatment of BCC.^[2,3] The histopathological subtype of BCC is, however,

correlated with treatment outcome^[4] and recommended treatment options therefore differ. Subtype, treatment efficacy and cosmetic outcome are important deciding factors for choosing the optimal care. The advent of non-invasive treatments as an alternative to surgical excision makes demands on the diagnostic methods. In spite of their invasive nature and possible lacking representativity,^[5] biopsies remain the gold standard for diagnosis of BCC; however, an optimal diagnostic tool would allow for accurate diagnosis and differentiation between specific skin cancer subtypes without leaving procedural scars. Non-invasive imaging techniques may provide a technologic solution to this diagnostic challenge.

Optical coherence tomography (OCT) is a non-invasive imaging method based on interferometry. It provides real-time images of the skin to a depth of 500-1500 μm with a resolution of $\leq 3\text{-}7.5\ \mu\text{m}$ (system dependent).^[6] Several morphologic OCT characteristics of BCC have been defined and evaluated,^[7-13] and OCT improves the diagnostic specificity for BCC.^[14,15] Although many studies have looked at OCT diagnosis of BCC,^[16-22] only few have explored the ability of OCT to discriminate between different BCC subtypes, possibly due to limited penetration depth of some OCT devices.^[10,23-25]

Based on conventional grey-scale OCT imaging, it has been speculated that an improved imaging of the vascular pattern may increase the diagnostic accuracy for BCC and its subtypes.^[10,24] Recent development of angiography-enabled OCT extends the applications of OCT from pure structural imaging to functional imaging of blood flow.^[26] The commercially available form, named Dynamic OCT (D-OCT; a variation in speckle variance OCT), enables in vivo imaging of skin microvasculature and has been validated for imaging of cutaneous blood flow.^[27] Initial reports on the potential utility of D-OCT for diagnosing different skin lesions, including skin cancer, have been published.^[28-34] This study explores D-OCT's ability to differentiate specific BCC subtypes based on microvascular and structural imaging.

2 | MATERIALS AND METHODS

Patients with primary BCC lesions referred for treatment at one of the three European clinical dermatology centres (ROS, MOD, AUG) and scanned with D-OCT from 21 August 2014 to 31 October 2016 were studied. Lesions were excluded if the pathology report did not include information about the histopathological subtype. The institutional review board of each centre approved the study (SJ-408), and all patients provided written informed consent in accordance with the principles of the Declaration of Helsinki. Patients were aged >18 years, and all lesions were D-OCT imaged prior to treatment. The subtypes found were as follows: sBCC, nBCC and iBCC. The subtype group of iBCC included both sclerosing and non-sclerosing variants. In four lesions, the pathology report showed BCC with pigmented characteristics. In this study, we considered pigmentation as a secondary change^[35] and these four lesions were therefore classified according to their primary histological subtype (nBCC = 2; sBCC = 1, iBCC = 1). The BCC lesions were histopathologically subtyped from specimens acquired by either

2-3 mm punch biopsy, shave/curettage biopsy (full lesion removed by curettage) or full surgical excision.

2.1 | Dynamic OCT—Image acquisition

All of the D-OCT images were acquired using a commercially available multibeam, Fourier domain OCT scanner (VivoSight Dx; Michelson Diagnostics, Kent, UK) with a centre wavelength of 1305 nm, optical resolution: $<7.5\ \mu\text{m}$ lateral; $<5\ \mu\text{m}$ axial, A-Line rate: 20 kHz and a scan area: 6 mm \times 6 mm. The in vivo imaging depth is 1000-1500 μm (tissue dependent) for structural OCT images and usually at least 500 μm for microcirculation images of the skin. The D-OCT images are presented in a cross-sectional and an en-face view. The blood flow data are acquired simultaneously with the structural OCT grey-scale data and displayed as an overlay in red colour. The technical specifications behind acquiring in vivo D-OCT images of the microcirculation have previously been described.^[28] Each BCC lesion was OCT scanned using a multislice modality of 120 B-scans (in the x-y plane) to form a 3D image block. A full scan took 30 seconds. No coupling medium was used, and the skin surface was not prepared prior to scanning. Images were obtained by placing the hand-held probe directly on the skin using a fitted plastic spacer for stability and carefully avoiding compression of the skin.

2.2 | Dynamic OCT – Analysis of microvasculature images

To evaluate the vascular features in the D-OCT images, we applied the terminology and guidelines described in the paper by Ulrich et al^[36] some of which include identifying prominent vascular shapes and evaluating the D-OCT images at three predefined skin depths of 150, 300 and 500 μm . As described in previous publications,^[31,37] we used specialized software (Michelson Diagnostics and University of Modena and Reggio Emilia, Modena, Italy) that detects the skin surface and allows the images to be viewed at desired depths below the skin surface. This "Fitted en-face" manoeuvre was performed as postprocessing and takes a maximum of ten seconds. For the purpose of this study, "Fitted en-face" D-OCT still-images from the three predefined image depths (150, 300 and 500 μm) were prepared and randomized, creating a D-OCT en-face study set of 294 images. Two of the authors (LT, NDC) performed blinded evaluations of the randomized study set assessing:

- (a) The presence of each vascular shape (Dots; Blobs; Coils; Lines; Curves; Serpiginous)
- (b) The presence of specific vascular characteristics:
 - (i) Branching vessels, ordinal scale:
 - No branching
 - Slightly present (1-5 arborizing vessels)
 - Highly present (≥ 5 arborizing vessels)
 - (ii) Vessels creating a circumscribed figure (CircumscribedAreas)
 - (iii) Vascular flare: a smudge red vascular appearance^[38] (Flare)
- (c) The vascular pattern (no pattern, mottle, mesh, cloud, chaos).

The observers collaborated on the evaluations, analysing and discussing the images jointly. Disagreements were settled by one of the senior authors (GJ, GP).

2.3 | Structural OCT – Analysis of structural images

For each BCC lesion, cross-sectional structural OCT scans (image “stacks” of 120 OCT images) were exported (TIFF format) creating a randomized study set of 98 structural OCT scans. Two observers (JO and LT) performed blinded evaluations using ImageJ (imagej.nih.hiv/ij/). We evaluated selected criteria in keeping with common OCT features previously described in studies of OCT of BCC.^[7,9,12,23,24] The included structural OCT criteria were as follows:

- Sharply demarcated hyporeflective ovoid structures located within the dermis (DemarcatedOvoid).
- Hyporeflective ovoid structures protruding from the epidermis (ProtrudingOvoid).
- Dark peripheral border at the margin of hyporeflective ovoid structures (DPB).
- Areflective cystic areas (ACS).
- Focal thinning of epidermis in relation to hyporeflective structures (FT).
- Fine hyper-reflective lines between adjacent nests (FHL).

Furthermore, the sizes of the hyporeflective structures (a) and (b) were estimated:

- Small: $\leq 350 \mu\text{m}$.
- Large: $> 350 \mu\text{m}$.

In both the vascular and structural evaluations, the observers were blinded to histopathological BCC subtype, clinical appearance and location of the BCC lesions.

2.4 | Statistics

2.4.1 | Analysis of the blinded observer evaluations

Prior to conducting any analyses, a statistical analysis plan was written (published online, <http://www.parkerinst.dk/>) and included pre-defined hypotheses. The patient and lesion characteristics were presented using descriptive statistics. The primary analyses consisted of investigating if there was an association with the BCC subtype and the microvascular or structural features. The outcome was coded as presence or non-presence of a specific BCC subtype, and the model was repeated for each of the three BCC subtypes.

It was necessary to simplify the originally planned models because many combinations of the covariates did not exist in the data. We calculated risk ratios and *P*-values based on chi-square tests. Stratified analyses were conducted at each depth for the microvascular features. As it was expected that 300 μm provided the best circumstances for image interpretation, analyses for this skin depth were considered primary. No correction for multiple testing was performed.

The robustness of our analyses was tested with several sensitivity analyses based on fixed and mixed effects logistic regression adjusting for age, gender and body location (sun exposed/relatively sun unexposed) as fixed factors, and patient as random factor.

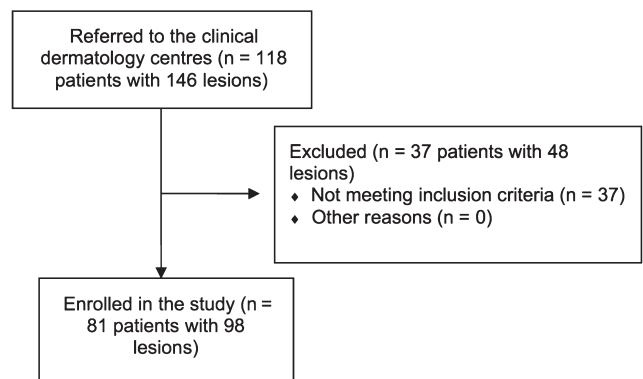
2.4.2 | Multiple correspondence analysis

Exploratory analysis using multiple correspondence analysis (MCA)^[39] was used to investigate the relationships between the different microvascular and structural features. The microvascular variables were analysed for each skin depth. All the structural and microvascular features were included with the levels, present and not present, except for vascular pattern. Diagnosis was included as supplementary variable.

All calculations were carried out in the statistical program R (version 3.3.3)^[40] using the packages lme4^[41] and FactoMinerR.^[42]

3 | RESULTS

Of 118 potentially eligible patients, we included a total of 81 patients with 98 BCC lesions. Patient characteristics are seen in Figure 1. The



Variable	(n = 81)
Gender, n females (%)	35 (43%)
Age, mean (SD)	67.0 (14.8)
Number of lesions	
1, n (%)	68 (84%)
2, n (%)	11 (14%)
3, n (%)	0 (0%)
4, n (%)	2 (2%)
Diagnosis	
sBCC, n (%)	18 (22%)
nBCC, n (%)	42 (52%)
iBCC, n (%)	15 (19%)
Combined, n (%)	6 (7%)
Centre	
ROS, n (%)	22 (27%)
MOD, n (%)	37 (46%)
AUG, n (%)	22 (27%)

FIGURE 1 Top: flow chart showing referred, excluded and included patients. Bottom: figure showing patient characteristics. BCC, basal cell carcinoma; iBCC, infiltrative BCC; nBCC, nodular BCC; n, number; SD, standard deviation; sBCC, superficial BCC. The “Combined” group under diagnosis means that there was more than one lesion type on the same patient

TABLE 1 Frequency of microvascular and structural OCT features of BCC, skin depth of 300 μm

	Superficial BCC (I = 27)	Nodular BCC (I = 55)	Infiltrative BCC (I = 16)
<i>Microvascular features (at 300 μm)</i>			
Dots (0-2), median (IQR)	2.0 (2.0; 2.0)	2.0 (2.0; 2.0)	2.0 (2.0; 2.0)
0: Not present (<3), n	0 (0%)	0 (0%)	0 (0%)
1: Slightly present (≥ 3 to <10), n	1 (4%)	5 (9%)	1 (6%)
2: Highly present (≥ 10), n	26 (96%)	50 (91%)	15 (94%)
Blobs (0-2), median (IQR)	0.0 (0.0; 0.0)	0.0 (0.0; 0.0)	0.0 (0.0; 0.0)
0: Not present (<3), n	21 (78%)	42 (76%)	13 (81%)
1: Slightly present (≥ 3 to <10), n	4 (15%)	12 (22%)	3 (19%)
2: Highly present (≥ 10), n	2 (7%)	1 (2%)	0 (0%)
Coils (0-2), median (IQR)	0.0 (0.0; 0.0)	0.0 (0.0; 1.0)	0.0 (0.0; 1.0)
0: Not present (<3), n	22 (81%)	34 (62%)	10 (63%)
1: Slightly present (≥ 3 to <10), n	4 (15%)	18 (33%)	6 (38%)
2: Highly present (≥ 10), n	1 (4%)	3 (5%)	0 (0%)
Lines (0-2), median (IQR)	1.0 (1.0; 2.0)	1.0 (1.0; 2.0)	1.0 (1.0; 1.0)
0: Not present (<3), n	2 (7%)	4 (7%)	3 (19%)
1: Slightly present (≥ 3 to <10), n	15 (56%)	31 (56%)	11 (69%)
2: Highly present (≥ 10), n	10 (37%)	20 (36%)	2 (13%)
Curves (0-2), median (IQR)	1.0 (1.0; 1.0)	1.0 (1.0; 2.0)	1.0 (1.0; 1.3)
0: Not present (<3), n	6 (22%)	8 (15%)	2 (13%)
1: Slightly present (≥ 3 to <10), n	15 (56%)	30 (55%)	10 (63%)
2: Highly present (≥ 10), n	6 (22%)	17 (31%)	4 (25%)
Serpiginous (0-2), median (IQR)	0.0 (0.0; 0.0)	0.0 (0.0; 1.0)	0.5 (0.0; 1.0)
0: Not present (<3), n	24 (89%)	30 (55%)	8 (50%)
1: Slightly present (≥ 3 to <10), n	3 (11%)	16 (29%)	6 (38%)
2: Highly present (≥ 10), n	0 (0%)	9 (16%)	2 (13%)
Arborizing (0-2), median (IQR)	0.0 (0.0; 0.0)	1.0 (0.0; 1.0)	0.0 (0.0; 1.0)
0: None, n	21 (78%)	25 (45%)	9 (56%)
1: Slightly present (≥ 1 to <5), n	5 (19%)	18 (33%)	4 (25%)
2: Highly present (≥ 5), n	1 (4%)	12 (22%)	3 (19%)
Circumscribed Areas, n	2 (7%)	13 (24%)	3 (19%)
Flare, n	13 (48%)	17 (31%)	4 (25%)
<i>The vascular pattern</i>			
No pattern, n	0 (0%)	1 (2%)	0 (0%)
Mottle, n	25 (93%)	43 (78%)	15 (94%)
Mesh, n	2 (7%)	9 (16%)	1 (6%)
Cloud, n	0 (0%)	0 (0%)	0 (0%)
Chaos, n	0 (0%)	2 (4%)	0 (0%)
<i>Structural features</i>			
<i>Demarcated Ovoid</i>			
0: Not present, n	17 (63%)	13 (24%)	5 (31%)
1: Primarily small, n	4 (15%)	29 (53%)	5 (31%)
2: Primarily mixed, n	1 (4%)	4 (7%)	1 (6%)
3: Primarily large, n	5 (19%)	9 (16%)	5 (31%)
<i>Protruding Ovoid</i>			
0: Not present, n	5 (19%)	26 (47%)	7 (44%)

(Continues)

TABLE 1 (Continued)

	Superficial BCC (I = 27)	Nodular BCC (I = 55)	Infiltrative BCC (I = 16)
1: Primarily small, n	13 (48%)	15 (27%)	5 (31%)
2: Primarily mixed, n	1 (4%)	0 (0%)	0 (0%)
3: Primarily large, n	8 (30%)	14 (25%)	4 (25%)
DPB	20 (74%)	39 (71%)	7 (44%)
ACS, n	8 (30%)	25 (45%)	7 (44%)
FT, n	11 (41%)	40 (73%)	6 (38%)
FHL, n	2 (7%)	8 (15%)	2 (13%)

BCC, basal cell carcinoma; DEJ, dermo-epidermal junction; iBCC, infiltrative BCC; IQR, Interquartile range; nBCC, nodular BCC; OCT, optical coherence tomography; I, number of lesions; sBCC; superficial BCC; DemarcatedOvoid, sharply demarcated hyporeflexive ovoid structures located within the dermis; ProtrudingOvoid, hyporeflexive ovoid structures protruding from the epidermis; DPB, dark peripheral border at the margin of hyporeflexive ovoid structures; ACS, areflexive cystic areas; FT, focal thinning of epidermis in relation to hyporeflexive structures; FHL, fine hyper-reflective lines between adjacent nests.

frequencies of the BCC subtypes were as follows: sBCC 28% (27 of 98), nBCC 56% (55 of 98) and iBCC 16% (16 of 98). The majority of sBCC lesions (74%) was located on relatively sun-unexposed body sites, while nBCC (60%) and iBCC (88%) were primarily located on sun-exposed areas. 76% of the lesions were sampled by full surgical excision, 8% by curettage/shave biopsy and 16% by 2 or 3 mm punch biopsy. Frequency of microvascular and structural OCT features of BCC subtypes at a skin depth of 300 μm is presented in Table 1. The frequency of microvascular OCT features of BCC subtypes at the remaining skin depths 150 and 500 μm is presented as in Tables S1 and S2.

3.1 | Microvascular D-OCT features

An overview of the estimates for the association between the BCC subtypes and microvascular and structural features at skin depths 150, 300 and 500 μm is presented as in Tables S3-S5. Looking at the simple vascular shapes (Dots, Blobs, Coils, Lines, Curves, Serpiginous), we only found significant associations with the BCC subtypes for serpiginous vessels and vascular lines. The risk of the subtype being nBCC was higher when serpiginous vessels were present at 300 and 500 μm ($RR_{300\mu\text{m}} = 1.44$, 95% CI [1.03, 2.01], $P = .043$; $RR_{500\mu\text{m}} = 1.59$, 95% CI [1.16, 2.17], $P = .014$). The lowest frequency of serpiginous vessels was found in sBCC (11%), and the risk of the subtype being sBCC was reduced by 78% ($RR_{300\mu\text{m}} = 0.22$, 95% CI [0.07, 0.66], $P = .001$) by the presence of serpiginous vessels. At a skin depth of 300 μm , the risk of iBCC, when observing highly present vascular lines (≥ 10 linear vessels), was significantly reduced, compared to the reference level ("Not present") ($RR_{300\mu\text{m}} = 0.19$, 95% CI [0.04, 0.96]). When comparing all three groups of presences (not, slightly, highly), the effect was, however, not significant ($P = .098$). Similar results were seen at a skin depth of 500 μm where the risk of iBCC was reduced by 68% by the presence of vascular lines, compared to the absence of lines ($RR_{500\mu\text{m}} = 0.38$, 95% CI [0.16, 0.90], $P = .031$). At a skin depth of 150 μm , the only prominent finding was a reduced risk of observing sBCC in the presence of vascular curves ($RR = 0.41$, 95% CI [0.20, 0.82], $P = .008$).

Looking at the specific vascular figures, seeing branching vessels at 300 μm significantly increased the risk of the subtype being nBCC ($RR_{300\mu\text{m}} = 1.53$, 95% CI [1.08, 2.18], $P = .016$), with 55% of nBCC lesions at this depth displaying some degree of branching/arborizing vessels. Furthermore, identification of branching vessels at 300 μm was associated with a reduced risk of observing sBCC ($RR_{300\mu\text{m}} = 0.37$, 95% CI [0.16, 0.83], $P = .008$). Significant RRs for branching/arborizing vessels were found neither at skin depth 150 μm nor at 500 μm . An increased risk of the subtype being nBCC was associated with the identification of vessels creating a circumscribed figure at depth 500 μm ($RR_{500\mu\text{m}} = 1.59$, 95% CI [1.15, 2.20], $P = .043$). Looking at the frequencies (Table S2), 18% of nBCC displayed this feature at 500 μm , compared to 4% and 6% for sBCC and iBCC, respectively. No significant RRs for CircumscribedAreas were found for any of the subtypes at depth 150 or 300 μm . Likewise, no significant RRs were found when identifying the feature, vascular flare for any of the subtypes at any depth. Lastly, we only found significant RRs for the vascular pattern, mottle. At a skin depth of 300 μm , the likelihood of nBCC was significantly reduced when mottling was seen ($RR_{300\mu\text{m}} = 0.65$, 95% CI [0.47, 0.90], $P = .043$). None of the other vascular patterns (mesh, cloud or chaos) differed significantly at any depth.

3.2 | Structural OCT features

An overview of the estimates for the association between the BCC subtypes and structural features is seen in supplementary table S4. The blinded evaluations showed that the risk of observing nBCC was significantly higher when identifying DemarcatedOvoid ($RR = 1.79$, 95% CI [1.13, 2.86], $P = .005$), and the risk of observing sBCC was only a third compared to the risk of the other subtypes when this structure was present ($RR = 0.33$, 95% CI [0.17, 0.63], $P = .001$). These demarcated structures appeared in 76% of the nBCC lesions compared to 37% and 69% in sBCC and iBCC, respectively. The size of DemarcatedOvoid in the nBCC lesions was primarily small in 53% of the cases, and the risk of nBCC when finding a small size of ovoid structures was also significantly increased ($RR = 2.05$, 95% CI [1.29,

3.27], $P = .006$). An increased risk of the subtype being nBCC was also found with FT (RR = 1.92, 95% CI [1.24, 2.97], $P = .001$).

In 81% of the sBCC lesions, we identified ProtrudingOvoid and the risk of observing sBCC, when finding this feature, was significantly increased (RR = 2.79, 95% CI [1.15, 6.73], $P = .011$). In 48% of the sBCC lesions, these protruding structures appeared primarily small and the association was statistically significant (RR = 2.99, 95% CI [1.19, 7.51], $P = .029$). Regarding the feature DPB, we found that the risk of the subtype being iBCC was reduced by 62% when identifying this feature (RR = 0.38, 95% CI [0.15, 0.92], $P = .028$). None of the RRs for the features ACS or FHL were found to be significant.

Looking at the robustness of the estimates for the association between the BCC subtypes and microvascular/structural features, the sensitivity analysis (logistic regression and mixed effects logistic regression with patient as random factor) adjusting for age, gender and location generally supported our findings (Tables S5-S7). In all cases, the sensitivity analysis showed the same tendencies as the initial analysis, and the significant findings, described in the sections above, were in most cases also significant in the sensitivity analysis. Overall, adjusting for age and location (sun exposed vs sun unexposed) led to most of the non-significant results in the sensitivity analysis in all of the BCC subtypes.

3.3 | Combining microvascular and structural features

The MCA showed that at a skin depth 300 μm , for the microvascular variables, the first two dimensions accounted for around 32% of the variability. The variables, Lines and Pattern were, however, removed because of too few observations. In the refitted MCA (Figure S1, MCA at 300 μm), the two-first dimensions accounted for around 37% of the variability, with the first dimension being highly dependent on the categories NoDemarcatedOvoid, NoProtrudingOvoid, Serpiginous and CircumscribedAreas, and the second dimension being highly dependent on NoCurves, Coils, CircumscribedAreas and NoCoils. The plot indicates that Branching was associated with Serpiginous, and that NoProtrudingOvoid was associated with ACS, FHL, FT and DemarcatedOvoid. As hypothesized, FT was associated with DemarcatedOvoid, and the subtype nBCC. When only considering the first dimension, CircumscribedAreas and Branching were associated with DemarcatedOvoid and the subtype nBCC, and Flare was associated with ProtrudingOvoid and subtype sBCC. Surprisingly, ProtrudingOvoid and NoDPB seemed to be associated. At 150 μm , the variables, Pattern, Flare, CircumscribedAreas and Coils were removed, and at 500 μm , the variables, Dots, Pattern and Blobs were removed (Figure S1, MCA 150 and 500). To a large degree, these plots showed the same associations as the MCA at depth 300 μm .

4 | DISCUSSION

Angiogenesis is important to the growth and metastasis of many cancers, including NMSC.^[43] Typically, angiogenesis is required

for tumors to grow beyond 1-2 mm in size because of increased metabolic demands.^[44] Vascular alterations therefore often become characteristic signatures of skin tumors.

Our findings indicate that the presence of serpiginous vessels at a skin depth of 300 and 500 μm increased the risk of observing nBCC. Furthermore, the identification of branching vessels at 300 μm was associated with a higher risk of the subtype being nBCC (Figure 2). In dermoscopy, the features branching/arborizing and serpiginous/serpentine vessels are described as closely related to NMSC,^[45] which was also found in our MCA (Figure S1). Branching/arborizing vessels are often described as the dermoscopic hallmark of nBCC^[45,46] and have also previously been identified in nBCC using en-face mode OCT (HD-OCT).^[25] The finding that branching/arborizing vessels in D-OCT were associated with a lower risk of observing the subtype sBCC (300 μm depth) is also supported by previous dermoscopy studies.^[46,47]

We found linear vessels at a skin depth of 500 μm to be associated with a lower risk of observing iBCC. At this depth, vascular lines were present in 93% of sBCC, 82% of nBCC and 62% of iBCC (Figure 3). In dermoscopy, short fine telangiectasia has been described as a feature of sBCC,^[47] however, the association of lines with a reduced risk of iBCC has to our knowledge not previously been reported. This may be due to the more limited imaging depth of dermoscopy only reaching

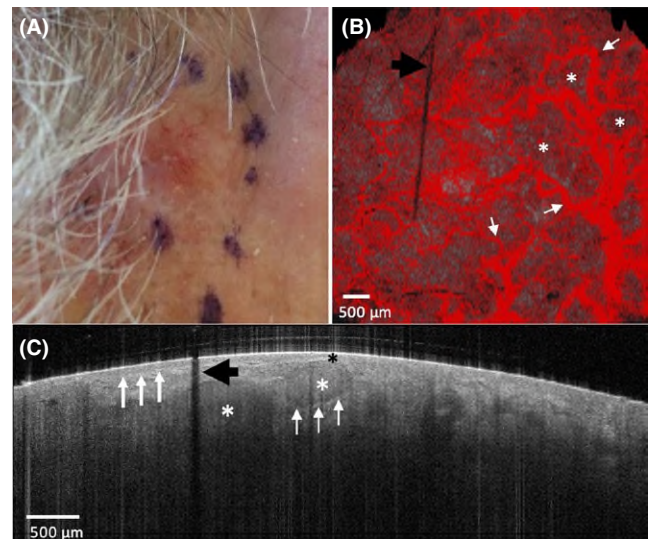


FIGURE 2 Illustration of the clinical, microvascular and structural features of a nodular basal cell carcinoma (nBCC). A, Clinical image of the nBCC lesion located on the preauricular area. B, Microvascular en-face D-OCT image (size: 6 mm \times 6 mm; skin depth 500 μm) of the same nBCC lesion as in (A). The asterisks mark CircumscribedAreas. The arrows mark examples of serpiginous vessels. Furthermore, branching/arborizing vessels are richly present. The thick black arrow marks a hair casting a shadow. C, Structural, cross-sectional OCT image (image size: 6 mm \times 2 mm; imaging depth: 800 μm) of the nBCC lesion. The white asterisks mark hyporeflexive ovoid structures corresponding to tumor nests; thin arrows mark dark peripheral borders at the margin of a hyporeflexive ovoid structure; the thick white arrows mark the dermo-epidermal junction; the black asterisk marks focal thinning of epidermis; the thick black arrow marks a hair casting a shadow

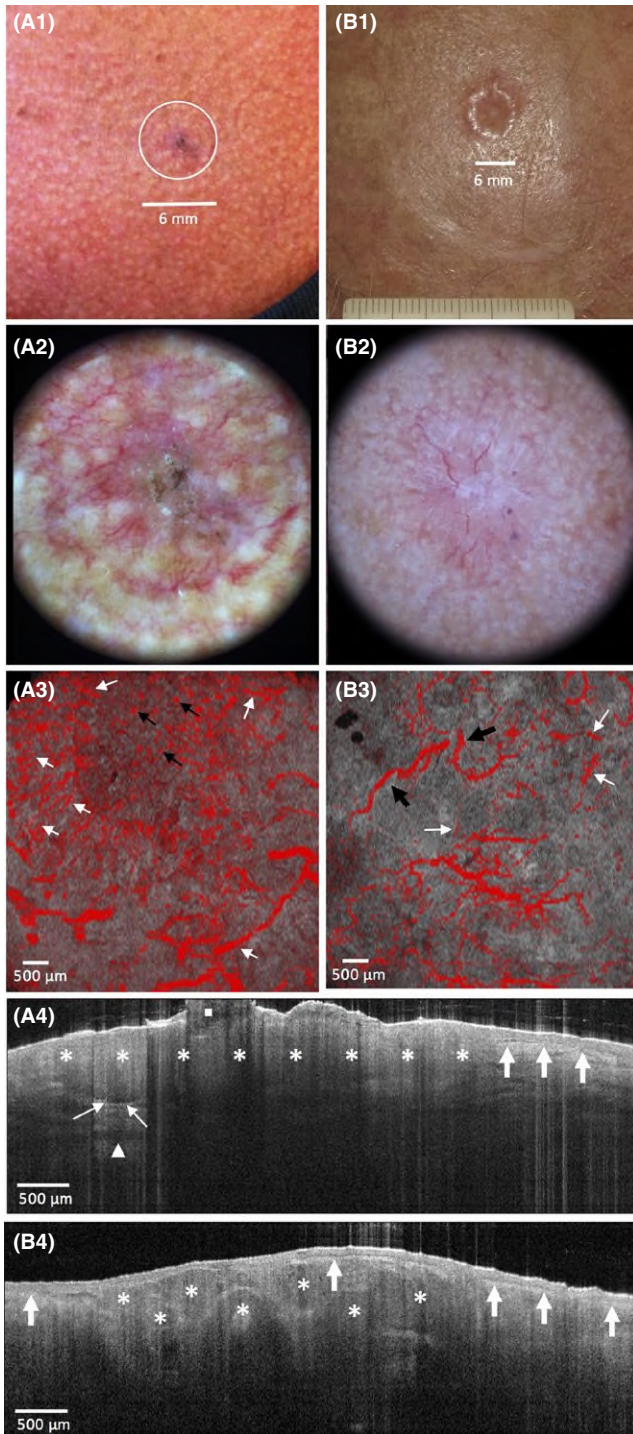


FIGURE 3 Illustration of the clinical, dermoscopic, microvascular and structural features of a superficial basal cell carcinoma (sBCC) (row (A)) and an infiltrative BCC (iBCC) (row (B)). A1, Clinical image of the sBCC lesion located on the chest. The white circle marks the exact area of the OCT scan. B1, Clinical image of the iBCC lesion located on the scalp. A2, Dermoscopic image (Handyscope® FotoFinder Systems GmbH, Bad Birnbach, Germany) of the sBCC lesion. B2, Dermoscopic image (Dermlite Photo 3Gen® LLC, San Juan Capistrano, CA, USA) of the iBCC lesion. A3, Microvascular D-OCT en-face image (size: 6 mm × 6 mm; skin depth 300 μm) of the sBCC lesion. The white arrows mark examples of vascular lines that are richly present. The black arrows mark vascular dots. The whole image has a predominantly mottle pattern. B3, Microvascular D-OCT en-face image (size: 6 mm × 6 mm; skin depth 300 μm) of the iBCC lesion. The white arrows mark examples of vascular lines that are sparsely present. The black arrows mark examples of serpiginous vessels. Branching/arborizing vessels are also sparsely present. A4, Structural, cross-sectional OCT image (image size: 6 mm × 2 mm; imaging depth: 1100 μm) of the sBCC lesion. The white aligned asterisks mark the hyporeflexive ovoid structure protruding from epidermis, corresponding to tumor nests; thin arrows mark the dark peripheral border at the margin of the hyporeflexive ovoid protruding nest—notice the so-called “window effect,” marked by the white triangle, which allows for an increase in imaging depth right below the tumor nest; the thick arrows mark the intact dermo-epidermal junction to the right in the image; the white square marks surface hyperkeratosis. B4, Structural, cross-sectional OCT image (image size: 6 mm × 2 mm; imaging depth: 1300 μm) of the iBCC lesion. The thick arrows mark the intact dermo-epidermal junction; the white asterisks mark the multiple sharply demarcated hyporeflexive ovoid structures in dermis, corresponding to tumor nests. The tumor nests are separated by hyper-reflecting lines of stroma

the superficial dermis, whereas D-OCT usually allows vascular imaging of the mid-dermis. At the superficial skin depth of 150 μm, we found a negative association between the presence of vascular curves and sBCC, possibly because angiogenesis represents a step in the development of more aggressive phenotypes.^[48] sBCC, being a non-aggressive subtype, may therefore displays a generally lower vessel count compared to the other subtypes and this may in turn explain why there are fewer visible vascular curves in the superficial parts of the sBCC. This connection between microvessel count and BCC aggressiveness has previously been reported.^[48]

We found the identification of vessels creating a circumscribed figure to be significantly associated with a higher risk of observing nBCC at a skin depth of 500 μm. Also, our MCA analysis showed associations between CircumscribedAreas, branching, DemarcatedOvoid and nBCC. This finding corresponds well with previous reports that primarily non-superficial BCCs display branching vessels coursing around and towards tumor nests;^[38] that angiogenesis is particularly evident at the boundary line between tumor and stroma^[48] and that the expression of vascular endothelial growth factor (VEGF) in BCC lesions is predominantly localized at the invading margin.^[43]

Based on the findings of a previous study using SIAscopy on NMSC, we had hypothesized that Flare, described as a smudge red appearance, was associated with sBCC.^[38] Although sBCC lesions in our study generally displayed the highest presence of Flare at all skin depths, we could not confirm this association in the primary statistical analysis. The MCA, however, showed an association between Flare, ProtrudingOvoid and sBCC, which corresponds well with the SIAscopy findings. Another hypothesis was the notion that a chaotic vascular pattern, characterized by disorder, would be associated with the iBCC subtype. We, however, found the chaotic pattern approximately equally distributed between all three subtypes (25%-37% at depth 500 μm). A recent D-OCT study on squamous cell carcinoma (SCC) spectrum lesions showed that chaos was the predominant pattern in

invasive SCC lesions (45.8%-62.5% at depth 500 μm).^[49] Studies on angiogenesis in NMSC lesions have found that tumor cells of BCC tend to show weak VEGF expression, whereas SCC displays more intense and widespread staining.^[43] The D-OCT findings may thus indicate that the chaotic pattern can be a feature in differentiating BCC and SCC lesions using D-OCT.

As hypothesized and previously reported in OCT studies, DemarcatedOvoid structures located within the dermis were positively associated with the subtype nBCC^[10] (illustrated in Figure 2 and Table S4) and ProtrudingOvoid from epidermis was positively associated with sBCC^[10,24] (illustrated in Figure 3 and Table S4).

One structural feature was associated with iBCC. We found that while DPB were equally present in sBCC and nBCC (74% and 71%, respectively), this characteristic was only present in 44% of the iBCC lesions and was significantly negatively associated with iBCC (illustrated in Figure 3). Previous OCT studies generally support the finding of a reduced presence of DPB in iBCC. von Braunmühl and colleagues found that DPB was one of the most frequent features in nBCC (94% [16 of 17]), but also identified that this feature was less frequently observed in sclerosing BCC than in the other subtypes (40% [2 of 5]).^[25] Cheng and colleagues defined this feature as solely visible at the inferior margin and found clefting (variety of DPB) to be one of the most useful positive predictors for sBCC (79% [69 of 87]).^[24] This group also found that clefting was less frequently observed in iBCC (29% [four of 14]). The histological correlate of the in vivo DPB in OCT images has been widely discussed. It has been suggested that this feature stems from peritumoral mucin;^[50] from peritumoral oedema^[12] or cellular peripheral palisading of BCC cells (accumulation of elongated nuclei orientated in the same axis).^[7] It might be that the OCT finding is associated with all three suggestions; however, in the histological literature, the *absence* of peripheral palisading and retraction is often described in iBCC subtypes^[51] and has generally been associated with more aggressive BCC subtypes.^[48] Regardless of the origin of this feature, DPB in OCT images seems to be an important in vivo OCT characteristic for differentiating iBCC aggressive subtypes from sBCC and nBCC.

5 | CONCLUSION

We identified various microvascular and structural D-OCT features that may aid non-invasive identification of BCC subtypes. This would allow clinicians to individualize and optimize BCC treatment as well as aid follow-up of non-surgical treatment.

5.1 | Limitations

The technical limitations of D-OCT have previously been described.^[27,31] We found some associations between microvascular features and BCC subtypes that were only significant at 500 μm . However, in some cases, D-OCT images at 500 μm can be challenging because of deteriorated signal/noise ratio at deeper skin levels. In this study, we did not rate the image quality and so we cannot report how

many of the D-OCT images were not optimal for evaluation. Despite this, the significant findings at 500 μm show that the microvascular features remain important to evaluate at this skin depth. Even though we included 98 lesions and the distribution of the BCC lesions subtypes corresponded to the distribution in the general population,^[1] we still only included a total of 16 iBCC cases. This is a small sample and increases the risk of error. Another limitation of our study is the sampling methods used. In 75% of the lesions (74 of 98), the histological diagnosis was based on full excision of the lesions; however, the remaining cases were sampled by either curettage/shave biopsy or punch biopsy. This can potentially have resulted in sampling errors, as the OCT field of view (6 mm \times 6 mm) is larger than the area of the punch biopsy and the curettage/shave biopsy may have missed important parts of the lesions. We acknowledge this limitation.

ACKNOWLEDGEMENTS

The project is part of the ADVANCE project that has received funding from the European Union's ICT Policy Support Program as part of the Competitiveness and Innovation Framework Program, grant agreement no: 621015. The manuscript reflects only the author's views, and the European Union is not liable for any use that might be made of information contained herein. Musculoskeletal Statistics Unit, the Parker Institute, Bispebjerg and Frederiksberg Hospital, is supported by a core grant OCAY-13-309 from the Oak Foundation.

CONFLICTS OF INTEREST

Martina Ulrich is stakeholder in CMB Collegium Medicum Berlin GmbH; clinical trials for Almirall, Biofrontera, Leo Pharma and Novartis; paid lectures for Almirall, Biofrontera, Galderma, Leo Pharma, Mavig GmbH, Michelson Diagnostics. Gregor B.E. Jemec has received honoraria from AbbVie, MSD, and Pfizer for participation on advisory boards, and grants from Abbvie, Actelion, Janssen-Cilag, Leo Pharma, Novartis and Regeneron for participation as an investigator, and received speaker honoraria from AbbVie, Galderma, Leo Pharma, and MSD. He has furthermore received unrestricted research grants from AbbVie, Novartis and Leo Pharma. Julia Welzel has received speaker honoraria from Almirall, Leo Pharma, Galderma, MSD and Novartis. She received honoraria from Almirall for participation in an advisory board on actinic keratosis. Giovanni Pellacani has received honoraria from MAVIG and Caliber for participation on advisory boards and teaching, and research grants from Abbvie, Leo Pharma, Novartis MSD for clinical studies. All other authors do not have any conflicts to declare.

AUTHOR CONTRIBUTIONS

All authors fulfilled criteria for authorship. The specific contributions to the study and manuscript of each of the authors were as follows: LT, NDC, JW, MU, GP and GJ designed the research study. LT, GJ, SC, SS, JW, NDC, GP contributed essential D-OCT images for the study. LT, GJ and SMN (supervised by Robin Christensen)

planned the statistical analysis, SMN performed the statistical analysis (supervised by Robin Christensen). LT, NDC and JO analysed the D-OCT images supervised by GP and GJ. BMN critically revised the histology reports and selected histology slides. LT wrote the paper, NDC, SMN, JO, SC, SS, BMN, JW, MU, GP and GJ critically revised the manuscript.

ORCID

Lotte Themstrup  <http://orcid.org/0000-0003-1368-1522>

Nathalie De Carvalho  <http://orcid.org/0000-0002-0823-5731>

REFERENCES

- [1] A. H. Arits, M. H. Schlangen, P. J. Nelemans, N. W. Kelleners-Smeets, *J. Eur. Acad. Dermatol. Venereol.* **2011**, *25*, 565.
- [2] K. M. McKay, B. L. Sambrano, P. S. Fox, R. L. Bassett, S. Chon, V. G. Prieto, *Br. J. Dermatol.* **2013**, *169*, 549.
- [3] C. Morton, R. M. Szeimies, A. Sidoroff, A. M. Wennberg, N. Basset-Seguín, P. Calzavara-Pinton, Y. Gilaberte, G. Hofbauer, R. Hunger, S. Karrer, P. Lehmann, S. Piaserico, C. Ulrich, L. Braathen, *Eur. J. Dermatol.* **2015**, *25*, 296.
- [4] H. W. Walling, S. W. Fosko, P. A. Geraminejad, D. C. Whitaker, C. J. Arpey, *Cancer Metastasis Rev.* **2004**, *23*, 389.
- [5] E. A. Wolberink, M. C. Pasch, M. Zeiler, P. E. van Erp, M. J. Gerritsen, *J. Eur. Acad. Dermatol. Venereol.* **2013**, *27*, 985.
- [6] S. Schuh, R. Kaestle, E. Sattler, J. Welzel, *Skin Res. Technol.* **2016**, *22*, 395.
- [7] A. J. Coleman, T. J. Richardson, G. Orchard, A. Uddin, M. J. Choi, K. E. Lacy, *Skin Res. Technol.* **2013**, *19*, 10.
- [8] T. Gambichler, I. Plura, P. Kampilafkos, K. Valavanis, M. Sand, F. G. Bechara, M. Stucker, *Br. J. Dermatol.* **2014**, *170*, 1358.
- [9] A. A. Hussain, L. Themstrup, G. B. Jemec, *Arch. Dermatol. Res.* **2015**, *307*(1), 1.
- [10] M. A. Boone, M. Suppa, G. Pellacani, A. Marneffe, M. Miyamoto, I. Alarcon, C. Ruini, R. Hofmann-Wellenhof, J. Malvehy, G. B. Jemec, V. Del Marmol, *J. Eur. Acad. Dermatol. Venereol.* **2015**, *29*, 1771.
- [11] J. Olsen, L. Themstrup, G. B. Jemec, *Ital. Dermatol. Venereol.* **2015**, *150*, 603.
- [12] T. Maier, M. Braun-Falco, T. Hinz, M. H. Schmid-Wendtner, T. Ruzicka, C. Berking, *J. Eur. Acad. Dermatol. Venereol.* **2013**, *27*, e97.
- [13] J. M. Olmedo, K. E. Warschaw, J. M. Schmitt, D. L. Swanson, *J. Am. Acad. Dermatol.* **2006**, *55*, 408.
- [14] M. Ulrich, T. von Braunmühl, H. Kurzen, T. Dirschka, C. Kellner, E. Sattler, C. Berking, J. Welzel, U. Reinhold, *Br. J. Dermatol.* **2015**, *173*, 428.
- [15] O. Markowitz, M. Schwartz, E. Feldman, A. Bienenfeld, A. K. Bieber, J. Ellis, U. Alapati, M. Lebowohl, D. M. Siegel, *J. Clin. Aesthet. Dermatol.* **2015**, *8*, 14.
- [16] M. Mogensen, T. M. Joergensen, B. M. Nurnberg, H. A. Morsy, J. B. Thomsen, L. Thrane, G. B. Jemec, *Dermatol. Surg.* **2009**, *35*, 965.
- [17] J. Olsen, L. Themstrup, N. De Carvalho, M. Mogensen, G. Pellacani, G. B. Jemec, *Photodiagn. Photodyn. Ther.* **2016**, *16*, 44.
- [18] C. Wahrlich, S. A. Alawi, S. Batz, J. W. Fluhr, J. Lademann, M. Ulrich, *J. Eur. Acad. Dermatol. Venereol.* **2015**, *29*, 1562.
- [19] A. A. Hussain, L. Themstrup, B. M. Nurnberg, G. Jemec, *Photodiagn. Photodyn. Ther.* **2016**, *14*, 178.
- [20] T. Gambichler, A. Orlikov, R. Vasa, G. Moussa, K. Hoffmann, M. Stucker, P. Altmeyer, F. G. Bechara, *J. Dermatol. Sci.* **2007**, *45*, 167.
- [21] M. Mogensen, B. M. Nurnberg, J. L. Forman, J. B. Thomsen, L. Thrane, G. B. Jemec, *Br. J. Dermatol.* **2009**, *160*, 1026.
- [22] S. A. Alawi, M. Kuck, C. Wahrlich, S. Batz, G. McKenzie, J. W. Fluhr, J. Lademann, M. Ulrich, *Exp. Dermatol.* **2013**, *22*, 547.
- [23] A. Meekings, S. Utz, M. Ulrich, A. Bienenfeld, N. Nandanani, J. Fisher, G. McKenzie, D. M. Siegel, E. Feldman, O. Markowitz, *J. Drugs Dermatol.* **2016**, *15*, 545.
- [24] H. M. Cheng, S. Lo, R. Scolyer, A. Meekings, G. Carlos, P. Guitera, *Br. J. Dermatol.* **2016**, *175*, 1290.
- [25] T. von Braunmühl, D. Hartmann, J. K. Tietze, D. Cekovic, C. Kunte, T. Ruzicka, C. Berking, E. C. Sattler, *J. Eur. Acad. Dermatol. Venereol.* **2016**, *30*, 1919.
- [26] C. L. Chen, R. K. Wang, *Biomed. Opt. Express* **2017**, *8*, 1056.
- [27] L. Themstrup, J. Welzel, S. Ciardo, R. Kaestle, M. Ulrich, J. Holmes, R. Whitehead, E. C. Sattler, N. Kindermann, G. Pellacani, G. B. Jemec, *Microvasc. Res.* **2016**, *107*, 97.
- [28] M. Ulrich, L. Themstrup, N. de Carvalho, M. Manfredi, C. Grana, S. Ciardo, R. Kastle, J. Holmes, R. Whitehead, G. B. Jemec, G. Pellacani, J. Welzel, *Dermatology* **2016**, *232*, 298.
- [29] O. Markowitz, M. Schwartz, S. Minhas, D. M. Siegel, *Dermatol. Online J.* **2016**, *22*, pii: 13030/qt7w10290r.
- [30] N. De Carvalho, S. Ciardo, A. Cesinaro, G. Jemec, M. Ulrich, J. Welzel, J. Holmes, G. Pellacani, *J. Eur. Acad. Dermatol. Venereol.* **2015**, *30*, e67.
- [31] L. Themstrup, S. Ciardo, M. Manfredi, M. Ulrich, G. Pellacani, J. Welzel, G. B. Jemec, *J. Eur. Acad. Dermatol. Venereol.* **2016**, *30*, 974.
- [32] S. Schuh, J. Holmes, M. Ulrich, L. Themstrup, G. B. Jemec, N. De Carvalho, G. Pellacani, J. Welzel, *Dermatol. Ther.* **2017**, *7*, 187.
- [33] H. C. Ring, L. Themstrup, C. A. Banzhaf, G. B. Jemec, M. Mogensen, *JAMA Dermatol.* **2016**, *152*.
- [34] A. S. Aldahan, L. L. Chen, R. M. Fertig, J. Holmes, V. V. Shah, S. Mlacker, V. M. Hsu, K. Nouri, A. Tosti, *Skin Appendage Disord.* **2017**, *2*, 102.
- [35] Y. Vantuchová, R. Čuřík, *SCRIPTA MEDICA (BRNO)* **2006**, *79*, 261.
- [36] M. Ulrich, L. Themstrup, N. de Carvalho, S. Ciardo, J. Holmes, R. Whitehead, J. Welzel, G. B. E. Jemec, G. Pellacani, *J. Eur. Acad. Dermatol. Venereol.* **2017**.
- [37] M. Manfredi, C. Grana, G. Pellacani, *Proceedings of the 11th Joint Conference on Computer Vision, Imaging and Computer Graphics Theory and Applications* **2016**, *4*, 234.
- [38] H. Tehrani, P. McArthur, M. Dalal, *Ann. Plast. Surg.* **2013**, *70*, 717.
- [39] M. Greenacre, *Stat. Methods Med. Res.* **1992**, *1*, 97.
- [40] R Core Team, R: A language and environment for statistical computing. Secondary R: A language and environment for statistical computing, <https://www.r-project.org/> (accessed: May 2017).
- [41] D. Bates, M. Mächler, B. Bolker, S. Walker, *J. Stat. Softw.* **2015**, *67*, 48.
- [42] S. Le, J. Josse, F. Husson, *J. Stat. Softw.* **2008**, *25*(1), 1.
- [43] K. E. Johnson, T. A. Wilgus, *J. Skin Cancer* **2012**, *2012*, 483439.
- [44] F. Hillen, A. W. Griffioen, *Cancer Metastasis Rev.* **2007**, *26*, 489.
- [45] I. Zalaudek, J. Kreuzsch, J. Giacomel, G. Ferrara, C. Catricala, G. Argenziano, *J. Am. Acad. Dermatol.* **2010**, *63*, 377. quiz 387-8.
- [46] A. Lallas, T. Tzellos, A. Kyrgidis, Z. Apalla, I. Zalaudek, A. Karatolias, G. Ferrara, S. Piana, C. Longo, E. Moscarella, A. Stratigos, G. Argenziano, *J. Am. Acad. Dermatol.* **2014**, *70*, 303.
- [47] I. Ahnslide, I. Zalaudek, F. Nilsson, M. Bjellerup, K. Nielsen, *Br. J. Dermatol.* **2016**, *175*, 751.
- [48] S. Staibano, A. Boscaino, G. Salvatore, P. Orabona, L. Palombini, G. De Rosa, *Hum. Pathol.* **1996**, *27*, 695.
- [49] L. Themstrup, G. Pellacani, J. Welzel, J. Holmes, G. B. E. Jemec, M. Ulrich, *J. Eur. Acad. Dermatol. Venereol.* **2017**, *31*, 1655.
- [50] M. Ulrich, J. Roewert-Huber, S. Gonzalez, F. Rius-Diaz, E. Stockfleth, J. Kanitakis, *J. Cutan. Pathol.* **2011**, *38*, 190.
- [51] M. Mackiewicz-Wysocka, M. Bowszyc-Dmochowska, D. Strzelecka-Weklar, A. Danczak-Pazdrowska, Z. Adamski, *Contemporary Oncol.* **2013**, *17*, 337.

SUPPORTING INFORMATION

Additional Supporting Information may be found online in the supporting information tab for this article.

Figure S1 Exploratory multiple correspondence analysis (MCA) factor maps used to investigate the relationships between the different microvascular and structural features at a skin depth of 150, 300 and 500 μm . In short, features that are positioned closely and laterally indicate association; features positioned centrally have very little influence on the analysis. "CircumscribedAreas": vessels creating a circumscribed figure; "Flare": vascular flare; "DemarcatedOvoid": sharply demarcated hyporeflective ovoid structures located within the dermis; "ProtrudingOvoid": hyporeflective ovoid structures protruding from epidermis; "DPB": dark peripheral border at the margin of hyporeflective ovoid structures; "ACS": areflective cystic areas; "FT": focal thinning of epidermis in relation to hyporeflective structures; "FHL": fine hyper-reflective lines between adjacent nests; "No" in front of an abbreviation means no presence of the specific structure.

Table S1 Lesion characteristics and frequency of microvascular features of BCC at 150 μm .

Table S2 Frequency of microvascular features of BCC at 500 μm .

Table S3 Crude estimates for the association between the type of BCC and microvascular features or structural features of BCC at 150 μm .

Table S4 Estimates for the association between the type of BCC and microvascular features or structural features of BCC at a skin depth of 300 μm .

Table S5 Estimates for the association between the type of BCC and microvascular features of BCC at 500 μm .

Table S6 Association between the type of BCC and microvascular features or structural features of BCC, for superficial BCC.

Table S7 Association between the type of BCC and microvascular features or structural features of BCC, for nodular BCC.

How to cite this article: Themstrup L, De Carvalho N, Nielsen SM, et al. In vivo differentiation of common basal cell carcinoma subtypes by microvascular and structural imaging using dynamic optical coherence tomography. *Exp Dermatol*. 2018;27:156–165. <https://doi.org/10.1111/exd.13479>